A Flux Parameterization Including the Effects of Capillary Waves and Sea State

MARK A. BOURASSA

Center for Ocean–Atmospheric Prediction Studies, The Florida State University, Tallahassee, Florida

DAYTON G. VINCENT

Department of Earth and Atmospheric Sciences, Purdue University, West Lafayette, Indiana

W. L. WOOD*

School of Civil Engineering, Purdue University, West Lafayette, Indiana

(Manuscript received 28 February 1997, in final form 26 May 1998)

ABSTRACT

An air–sea interaction model that includes turbulent transport due to capillary waves (surface ripples) is developed. The model differs from others in that the physical premises are applicable to low wind speeds (10-m wind speed, $U_{10} < 5$ m s^{-1}) as well as higher wind speeds. Another new feature of the model is an anisotropic roughness length, which allows a crosswind component of the stress to be modeled. The influence of the angle between the mean wind direction and the mean direction of wave propagation is included in the anisotropic roughness length.

Most models are not accurate at low wind speeds and tend to underestimate fluxes in low wind speed regions such as the tropical oceans. Improvements over previous models are incorporated in the momentum roughness length parameterization. In addition, the dimensionless constant in the relationship between the capillary wave component of momentum roughness length and friction velocity is reevaluated using both wave tank data and field data. The new value is found to be 0.06, a factor of 3 smaller than the original estimate of 0.18. Modeling the influence of capillary waves is shown to improve the accuracy of modeled surface fluxes and drag coefficients. Several sets of tropical observations are used to examine mean increases in modeled fluxes due to capillary waves. The changes in latent heat fluxes are compared to proposed increases due to convective overturning (sometimes called gustiness) and are found to be larger by a factor of 4. For $U_{10} < 7$ m s^{-1}, the mean estimates for tropical fluxes of momentum and latent heat are found to increase by 0.004 N m^{-2} and 6 W m^{-2}.

1. Introduction

Evaporation at low latitudes is a very important component of many large-scale phenomena, such as the Madden–Julian oscillation, El Niño, the tropical general circulation, poleward transport of heat, and climate change. A large portion of this evaporation takes place over warm subtropical waters at relatively low wind speeds (10-m wind speed, U_{10}, < 7 m s^{-1}). This vapor is usually transported away from the subtropics and is ultimately responsible for some of the clouds and precipitation that occur at higher latitudes, as well as persistent cloud cover in the deep Tropics (e.g., in the intertropical convergence zone). Accurate estimates of moisture transport require accurate estimates of surface evaporation and stress. Inaccurate estimates can cause significant errors in long-term weather forecasts and in climate models.

An improved air–sea interaction parameterization is developed, herein, by considering the effects of capillary waves, which in the absence of steep long waves have been shown to dominate the generation of turbulence (Wu 1968). The conditions for which wind-induced ripples exist are also considered: for conditions of local equilibrium between the wind and the waves, there is a wind speed (referred to as the capillary cutoff) below which waves will not exist. Preliminary, theory-based estimates of a capillary wave–related mean increase in evaporation of 20 W m^{-2} over the tropical Pacific indicated that capillary waves are of great importance (Bourassa 1993); however, this large mean increase in predicted fluxes was not consistent with observations provided by Frank Bradley (1994, personal communication; also see Bradley et al. 1991; Bradley

* Deceased.

Corresponding author address: Mark A. Bourassa, Center for Ocean–Atmospheric Prediction Studies, The Florida State University, Tallahassee, FL 32306.
E-mail: bourassa@coaps.fsu.edu

et al. 1993). A reevaluation of our assumptions revealed that a dimensionless constant in the momentum roughness length parameterization for capillary waves (Wu 1968) had been overestimated, causing the influence of capillary waves to be overestimated. The correction to the roughness length parameterization results in a superior match to observations (Clayson et al. 1996), and the influence of capillary waves is significant for $U_{10} < 7$ m s^{-1}.

The physics of the model described herein explains the shape of relation for the drag coefficient, $C_D(U_{10})$, determined during several open ocean experiments (Dupuis et al. 1997). The key considerations for $U_{10} < 7$ m s^{-1} are stress related to capillary waves, and a roughness length modification (related to sea state) that puts roughness length in the frame of reference of the mean surface current. Another improvement is a break from the usual assumption that mean wind, waves, and currents all move parallel to each other. The last two considerations offer an explanation for the wide scatter of individual observations from mean $C_D(U_{10})$ observed in the open oceans, as well as an explanation for changes that have been observed when winds shift direction (Geernaert 1988; Rieder et al. 1994; Donelan et al. 1997). It is expected that air–sea interaction models with these considerations will be of use when ocean and atmospheric models are coupled in a manner that considers currents, sea state (waves), and boundary layer winds.

2. Theory

The downward momentum flux ($\boldsymbol{\tau}$) is defined in terms of the ''surface'' friction velocity ($\mathbf{u}_*$):

$$\boldsymbol{\tau} = \rho \mathbf{u}_* |\mathbf{u}_*|, \tag{1}$$

where ρ is the density of the air and bold type indicates a vector quantity. It has long been accepted that the vertical differences between near-surface values of mean wind speed (U) increase approximately logarithmically with height (z), as given by:

$$\mathbf{U}(z) - \mathbf{U}_s = \frac{\mathbf{u}_*}{\kappa}\left[\ln\left(\frac{z}{z_0} + 1\right) + \varphi(z, z_0, L)\right], \tag{2}$$

where $\mathbf{U}_s$ is the mean ocean surface current, κ is von Kármán's constant, z_0 is the momentum roughness length, φ is an atmospheric stability term, L is the Monin–Obukhov scale length, and $\mathbf{U}$, $\mathbf{U}_s$, and $\mathbf{u}_*$ are assumed to be parallel. The friction velocity can be obtained from Eq. (2), given L and a relation between roughness length and friction velocity, such as Charnock's (1955) relation. The height over which (2) applies ranges from approximately three times the significant wave height (Large et al. 1995) to between 4% and 10% of the surface layer (Carl et al. 1973; Pielke 1984). The surface current serves as the frame of reference for the wind velocity (analogous to a stationary frame of reference over solid surfaces). The consequences of this rather arbitrary choice of reference frame will be discussed in detail when the new model is developed (section 3). The locally induced surface current is usually very small compared to U_{10} (Wu 1975), and it can be treated as negligible. In contrast, the surface current induced by large-scale circulation can be significant (Chou 1993), but it cannot be parameterized in terms of local variables. Traditionally $\mathbf{U}_s$ is dropped from Eq. (2), but it will be retained herein because it provides a uniform frame of reference, and the surface drift due to large-scale circulation is considered in most of the field data used to develop or test the proposed model.

The upward fluxes of heat and moisture (H and E) are defined in terms of u_* and the analogous terms (respectively, θ_* and q_*) in the vertical distributions of potential temperature and moisture:

$$H = -C_p \rho \theta_* u_*, \tag{3}$$

$$E = -L_v \rho q_* u_*, \tag{4}$$

where C_p is the heat capacity of air, and L_v is the latent heat of vaporization. The vertical distributions of potential temperature (θ) and specific humidity (q) have a logarithmic form similar to the momentum profile:

$$\theta(z) - \theta_s = \frac{\theta_*}{k_\theta}\left[\ln\left(\frac{z}{z_{0\theta}} + 1\right) + \varphi_\theta(z, z_{0\theta}, L)\right]; \quad \text{and} \tag{5}$$

$$q(z) - q_s = \frac{q_*}{k_q}\left[\ln\left(\frac{z}{z_{0q}} + 1\right) + \varphi_q(z, z_{0q}, L)\right], \tag{6}$$

where the variables are similar to those in Eq. (2), except that terms with the subscript θ relate to potential temperature and those with a subscript q relate to moisture. The von Kármán constants were set at $\kappa = \kappa_\theta = \kappa_q = 0.40$, which is consistent with the stability functions and roughness length parameterizations used herein.

a. Atmospheric stability parameterization

The flux parameterization discussed herein was developed in parallel with a sea state model that required that the atmospheric stability terms be well behaved when the reference height (z) approaches the wave height. Consequently, we use Benoit's (1977) parameterizations for an unstable atmosphere, which is a slightly more detailed solution than the usual Businger–Dyer parameterizations (Dyer 1974; Liu et al. 1979). For a stable boundary layer, the Beljaars and Holtslag (1991) parameterization is applied. The Monin–Obukhov scale length is calculated as described by Liu et al.

At very low wind speeds, several of the assumptions related to a shear stress break down. One problem is that a 10-m reference height is well above this layer, which implies that convection induces a significant frac-

tion of the mixing at the reference height. Another problem is that, contrary to an assumption typically used to derive a log-wind profile, wind perturbations can apply more surface stress than the mean wind. Schumann (1988) has developed a rather complex scheme for accounting for these effects. A simple approximation of Schumann's work produces reasonable results (Godfrey and Beljaars 1991; Fairall et al. 1996a,b) for determining an effective wind speed (U'):

$$U' = [(U - U_s)^2 + \gamma w_*^2]^{1/2}, \tag{7}$$

where

$$w_* = (-u_* b_* Z_{\rm bl})^{1/3}, \tag{8}$$

$$b_* = g[(1 + 0.61q)\theta_* + 0.61q_*\theta]/\theta_v, \tag{9}$$

γ is a constant of order one, $-b_*u_*$ is the buoyancy flux, $Z_{\rm bl}$ is the height of the convective boundary layer, g is gravitational acceleration, and θ_v is the virtual potential temperature. Schumann suggested that $\gamma = 0.7$; however, a value of $\gamma = 1.25$, suggested by Fairall et al. (1996a,b) for tropical oceans is used herein. The value of $Z_{\rm bl}$ is rarely known and when not reported it is assumed to be a constant equal to 1000 m (Bradley et al. 1991), which is typical for the Tropics. The magnitude of the increase in latent heat fluxes due to wind perturbations will be compared (section 8a) to the increase due to capillary waves.

b. Roughness length parameterizations

Both field and wind tunnel observations show that, for conditions of local wind–wave equilibrium, there is a low wind speed cutoff below which surface waves do not exist. This is usually observed in the range of 1–4 m s^{-1} (Ursell 1956). The sea surface is aerodynamically smooth for wind speeds less than this cutoff and is aerodynamically rough for speeds greater than the cutoff.

1) AERODYNAMICALLY SMOOTH REGIME

Aerodynamically smooth surfaces, which are amenable to laboratory experiments, have been found to have different roughness lengths for momentum, potential temperature, and water vapor (Nikuradse 1933; Kondo 1975; Brutsaert 1982):

$$z_0 = \frac{0.11\nu}{u_*}, \tag{10}$$

$$z_{0\theta} = \frac{0.40\nu}{u_*}, \tag{11}$$

$$z_{0q} = \frac{0.62\nu}{u_*}. \tag{12}$$

Smith (1988, 1989) suggests that waves have no direct effect on the functional form of roughness lengths for temperature and moisture; thus, the above temperature and moisture roughness lengths apply to both aerodynamically smooth and rough surfaces.

2) AERODYNAMICALLY ROUGH REGIME

For $U_{10} > 7$ m s^{-1}, the momentum roughness length is well described with gravity waves as roughness elements. Roughness elements are the objects causing the turbulence; they have heights much larger than the roughness length. In the case of gravity waves, the roughness elements that generate most of the turbulence appear to be the short waves (Banner and Phillips 1974; Dobson et al. 1994). The additional physics considered in our roughness length parameterization (hereafter referred to as BVW) will be discussed in comparisons to fluxes and drag coefficients based on the physics considered in several dimensionally sound roughness length parameterizations, as well as comparisons to several sets of observations. Charnock's (1955) relation is the most widely used roughness length parameterization:

$$z_0 = au_*^2/g, \tag{13}$$

where a is an empirically derived constant. In near-shore environments $a \approx 0.0185$ (Wu 1980); however, in open ocean observations $a \approx 0.011$ (Smith 1988; Dobson et al. 1994) is usually found to be smaller than in the near-shore observations. Recently, there have been several examinations of the dependence of Charnock's constant on sea state (Kusaba and Masuda 1988; Geernaert et al. 1990; Toba et al. 1990; Perrie and Toulany 1990; Maat et al. 1991; Smith et al. 1992; Yelland et al. 1998), for which Smith et al. found

$$z_0 = \frac{0.48}{w_a}\frac{u_*^2}{g}, \tag{14}$$

where $w_a = c_p/u_*$ is the wave age, and c_p is the phase speed of the dominant waves. These analyses are restricted to the subset of observations without significant swell (long gently sloping waves generated by distant events). The drag coefficients and stresses determined from this subset are approximately 20% larger than the open ocean results. A simple inverse wave age relationship (14) does not adequately describe the variation in $C_D(U_{10})$ observed when swell is present (Smith et al. 1992; Dobson et al. 1994). Dobson et al. suggest that a model with two horizontal dimensions is required to resolve the complexities introduced by swell.

Both of the above roughness length parameterizations (Smith 1988; Smith et al. 1992) are based upon field observations at $U_{10} > 6$ m s^{-1} and do not adequately model the processes that govern low wind speeds. Smith (1988) attempted to rectify this shortcoming by assuming that the roughness length for an aerodynamically smooth surface (Nikuradse 1933; Kondo 1975; Brutsaert 1982) could be added linearly to the gravity wave roughness length:

TABLE 1. The physical considerations in the roughness length parameterizations of Charnock (1955), Smith et al. (1992), Smith (1988), and the model described herein (BVW).

	Charnock	S92	S88	BVW
Gravity waves	yes	yes	yes	yes
Capillary waves	no	no	no	yes
Aerodynamically smooth surface	no	no	yes	yes
Wave age	no	yes	no	yes
Two horizontal dimensions	no	no	no	yes

$$z_0 = \frac{0.11\nu}{u_*} + a\frac{u_*^2}{g}. \tag{15}$$

A summary of the physics considered in these parameterizations is provided in Table 1.

3. The BVW flux model

There are three key differences between the BVW flux model and other flux models. One improvement is the inclusion of capillary waves as roughness elements (objects that interact with the airflow to generate turbulence) for aerodynamically rough surfaces. Another improvement is the provision that the wind, stress, surface currents, and direction of wave propagation need not always be assumed to be parallel. This consideration is particularly important at low wind speeds in the presence of swell (very long waves), where the stress vector has been observed to be closer to the direction of wave propagation than the wind direction (Fairall et al. 1996a). It has recently been observed that the angle between the mean directions of wind and swell propagation has a systematic influence on open ocean drag coefficients (Donelan et al. 1997). Both of these considerations increase the magnitude of low wind speed fluxes. The last improvement is the distinction between aerodynamically smooth and rough regimes.

a. Capillary wave roughness length

For high winds, the momentum roughness length is well described with gravity waves as roughness elements: however, at low wind speeds or short fetches, capillary waves can dominate the generation of turbulence (Wu 1968). These waves are much shorter than the gravity waves; however, they are much steeper and more densely packed. Wu (1968, 1994) has suggested that capillary waves contribute to turbulent transfer and hence to the momentum roughness length. This reasoning is supported by Byshev and Kuznetsov's (1969) observations that, at similar wind velocities, turbulent momentum fluxes were much greater when capillary waves were observed. Wu's (1968) observations showed that roughness length associated with capillary waves decreases monotonically as wind speed increases. For similar wind speeds, the roughness length associated with capillary waves was larger than the roughness length for aerodynamically smooth surfaces. On the basis of dimensional analysis, Wu suggested that the momentum roughness length for capillary waves was related to friction velocity and the kinematic surface tension (σ/ρ_w, where σ is the surface tension, ρ_w is the density of water):

$$z_0 = \frac{b\sigma}{u_*^2\rho_w}, \tag{16}$$

where b is an empirically derived constant that he determined to be approximately 0.18.

We propose that roughness length for combined gravity and capillary waves can be approximated as the root-mean-square sum of the roughness lengths. There have been many investigations into the relationship between the characteristics of roughness elements and the corresponding roughness length (e.g., Lettau 1969; Kondo and Yamazawa 1985). Kondo and Yamazawa's findings support an additive rule; however, the exact nature of the weighting remains uncertain. The roughness length is likely to be either the sum of the components (z_{0g} and z_{0c}) or the rms sum of the components. There is little difference between the two sums except when $z_{0g} \approx z_{0c}$ ($6 < U_{10} < 8$ m s^{-1}):

$$z_{0g}^2 + z_{0c}^2 = (z_{0g} + z_{0c})^2 - \frac{2ab\sigma}{\rho_w g}. \tag{17}$$

In either case, the total roughness length is usually approximately equal to the sum of the component roughness lengths. The shape of $C_D(U_{10})$ for the rms sum is qualitatively similar to an empirically derived parameterization (Large et al. 1994), which is a synthesis of Large and Pond's (1981) 25 years of ocean weather ship observations, and a GCM-based estimate (Trenberth et al. 1989) of $C_D(U_{10})$ for low wind speeds. The BVW $C_D(U_{10})$ for wind–wave equilibrium is 10%–20% greater than that of Large et al. (1994) and other open ocean observations (Smith 1980; Anderson 1993; Dobson et al. 1994; Dupuis et al. 1997); it will be shown that these differences are consistent with the influence of sea state.

There is a further complication to the above solution. Roughness length [Eq. (2)] is highly dependent on the Newtonian frame of reference. For a solid surface the frame of reference is obviously earth relative ($U_s = 0$). For aerodynamically rough fluids, it is not clear that the mean surface current is the appropriate reference velocity. In practice, a frame of reference is chosen, and roughness length is determined for that frame of reference. The complication is that the frame of reference for capillary waves observed in a wave tank could differ from the frame of reference of capillary waves superimposed on a field of gravity waves in the open ocean.

We propose that the momentum roughness length for an aerodynamically rough surface is the weighted rms sum of the roughness lengths for capillary waves and for gravity waves:

$$z_0 = \left[\left(\beta_c \frac{b\sigma}{u_*^2 \rho_w}\right)^2 + \left(\beta_g \frac{0.48}{w_a}\frac{u_*^2}{g}\right)^2\right]^{0.5}, \quad (18)$$

where the β terms are weights based on several physical considerations. This parameterization does not contradict previous results for high winds: at high wind speeds, the capillary wave roughness is insignificant in comparison to gravity wave roughness. The weights will account for the above-mentioned frame of reference (section 3c) as well as modifications due to directions of wave propagation and surface currents that are nonparallel to the wind direction (section 3b).

b. Anisotropic roughness length

It is difficult to describe the parameterization for the weights without first describing the log-wind relation in vector form. A scalar form has been commonly used because the problem is greatly simplified when all the mean horizontal motion vectors were considered parallel. In such a case, a single roughness length (for the vertical plane that was parallel to the wind) could be used to model the mixing and the wind profile. When the mean horizontal flows are not all parallel, another roughness length is required to describe mixing due to the cross-flow.

We propose that the general form of the log-wind profile for a rough surface becomes

$$[\mathbf{U}(z) - \mathbf{U}_s] \cdot \hat{\mathbf{e}}_i = \frac{\mathbf{u}_* \cdot \hat{\mathbf{e}}_i}{\kappa}\left[\ln\left(\frac{z}{z_{0_i}} + 1\right) + \varphi(z, z_{0_i}, L)\right], \quad (19)$$

where $\hat{\mathbf{e}}_i$ are orthogonal horizontal basis vectors (e.g., $i = 1$ for flow parallel to the direction of wave propagation, and $i = 2$ for cross-flow), and z_{0_i} are roughness length components for the corresponding basis. This approach requires reconsideration of the meaning of u_* in wave age and the roughness lengths. There are few plausible interpretations, the number of which can be reduced by two limitations: the roughness length must be positive, and the magnitude of stress should be invariant to the choice of orthogonal basis vectors. The second constraint is difficult to apply, so the limiting cases of the stress associated with individual roughness components (z_{0c} and z_{0g}) are used to reinterpret the roughness length parameterizations. For z_{0g} there are two cases that meet this requirement:

$$z_{0g_i} = \frac{0.48}{w_a}\frac{\mathbf{u}_* \cdot \mathbf{u}_*}{g}, \quad \text{and} \quad (20)$$

$$z_{0g_i} = \frac{0.48}{w_a}\frac{|\mathbf{u}_*||\mathbf{u}_* \cdot \hat{\mathbf{e}}_i|}{g}. \quad (21)$$

In the first case z_{0g} is invariant to direction. Equation (19) shows that z_0 can be independent of bases only when $(U - U_s)/u_*$ is independent of wind speed, which is inconsistent with the vast majority of observations. Consequently, z_0 must be anisotropic.

The roughness length in (21) also has the advantage of being consistent with a zero-magnitude stress component when there is no wind shear in that component. That is, the roughness length approaches zero as the wind shear and stress both approach zero. Additional support for this form comes from its similarity to the stress vector (1): $|\mathbf{u}_*|\mathbf{u}_* \cdot \hat{\mathbf{e}}_i$ are the components of stress parallel to $\hat{\mathbf{e}}_1$ and $\hat{\mathbf{e}}_2$. The form of Eq. (21) is physically more reasonable; consequently, it is used in the BVW roughness length.

Similar reasoning is used to interpret the roughness length components for capillary waves. Again the same two forms meet the requirement of invariance to the choice of basis vectors; the form similar to (21) is chosen for similar reasons:

$$z_{0c_i} = \frac{b\sigma}{\rho_w |\mathbf{u}_*||\mathbf{u}_* \cdot \hat{\mathbf{e}}_i|}. \quad (22)$$

In the case of capillary waves, an infinite roughness length corresponds to nonexistent wind shear and a zero stress component.

The concept of wave age is not one that can easily be thought of as bases or frame of reference dependent: wave age describes the relation between the dominant long waves and the stress applied to waves:

$$w_{a_i} = \mathbf{u}_* \cdot \hat{\mathbf{e}}_i / c_{p_i}. \quad (23)$$

This form of wave age implies that winds perpendicular to the direction of wave propagation, and waves induced by these winds, do not directly affect the sea state related to swell. In the absence of both swell and changing winds, the wind-induced waves will propagate parallel to the wind, and this definition of wave age will not differ from the traditional scalar form.

c. Weights for roughness lengths

Traditionally, z_{0g} is considered determined for the frame of reference moving with the surface current. Consequently, there is no frame of reference adjustment to β_g. However, if swell is present, and if it is considered in the roughness for the direction it is propagating, then gravity wave roughness is either that of the swell (z_{0_1}) or that of gravity wave moving perpendicular to the swell (z_{0_2}). That is, airflow parallel to the ''crests'' of the swell will not ''feel'' the swell as gravity wave roughness elements. Neither the Smith et al. (1992) nor BVW parameterization of roughness length considers complications such as multiple sources of swell. Such consideration can be added to the BVW model; several prerequisite considerations are discussed in section 8. The wave field assumptions used herein are an improvement over the common assumptions in that they consider roughness elements for airflows that are parallel and perpendicular to swell.

Any stress, due to an airflow component perpendicular to the direction of swell propagation, is related to relatively short wavelength wind-induced waves. The waves in the cross-flow direction are assumed to be in local equilibrium with the wind. Winds tend to be approximately parallel to the direction of wave motion except at low wind speeds; therefore, the phase speed for the perpendicular component of the flow is generally small in comparison to the phase speed of the dominant waves. This assumption is most easily conceptualized when $\hat{\mathbf{e}}_1$ is parallel to the direction of wave propagation for the dominant wave, and when $\hat{\mathbf{e}}_2$ is perpendicular to $\hat{\mathbf{e}}_1$ (the positive direction is consistent with a right-handed coordinate system, where the vertical axis is positive in the upward direction). This assumption results in one wave age for the dominant waves, and a smaller wave age for the cross-flow.

The alignment (i.e., anisotropy) of open-ocean capillary waves is not well known. In the open ocean, capillary waves are often superimposed on a field of gravity waves. Only those capillary waves that are elevated into the wind stream, which is aerodynamically joined to the water surface (i.e., the areas where flow separation has not occurred), will contribute to the stress. Therefore, the velocity frame of reference is shifted by the mean horizontal motion of the surface of this elevated portion of the wave. This shift in velocity ($\mathbf{U}_c$) cannot exceed the orbital velocity of the supporting gravity waves (i.e., the velocity of ''particles'' moved by wave motion). Correcting $\mathbf{U}$–$\mathbf{U}_c$–$\mathbf{U}_s$ to a $\mathbf{U}_s$ frame of reference is equivalent to modifying β_c:

$$\beta_{c_i} = \exp[-\kappa \mathbf{U}_c(\hat{\mathbf{c}}_p \cdot \hat{\mathbf{e}}_i)/u_{*i}]. \quad (24)$$

If flow separation occurs then there should be a positive value for U_c; however, there are no observations on which to base the fraction of the mean orbital velocity that corresponds to the frame of reference modification. The orbital speed of gravity waves (U_{orb}) is

$$U_{\text{orb}} = \pi H_s/T_p. \quad (25)$$

The significant wave height (H_s) and the period of the dominant waves (T_p) are contained in the San Clemente Ocean Probing Experiment (SCOPE; Fairall et al. 1996a) dataset. These observations were taken from the Scripps Institute Floating Instrument Platform: R/P *FLIP*, in deep water off the California coast. The stress components parallel to the wind were measured with a sonic anemometer, and wave characteristics were measured with pressure sensors located 1.7 m below the mean surface. Significant wave height and period can also be estimated by solving Toba's two-thirds law (Toba et al. 1990) simultaneously with the phase relation for water waves. Wave characteristics estimated through this approach are similar to those determined from a Sverdrup–Munk–Bretshneider nomogram (M. A. Bourassa et al. 1998, submitted to *J. Phys. Oceanogr.*). The frame of reference correction ($\mathbf{U}_c$) must be a fraction of the orbital speed. Fractions from zero to one were tested using the SCOPE observations, and it was found that fractions less than 0.45 resulted in poorer correlations between observed and modeled drag coefficients. Observations covering a wider range of sea states will be needed to examine this fraction for a dependency on sea state. It is arbitrarily assumed that U_c is equal to be half the orbital velocity. The frame of reference corrections will be shown (in section 5) to have a role in changes of $|\boldsymbol{\tau}|$ with direction of wave propagation.

d. Capillary cutoff

The capillary cutoff is used to determine if wind-induced capillary waves are present and contributing to the surface roughness. We have assumed that surface waves do not exist if the modeled phase speed of the dominant waves is less than the minimum phase speed ($c_{p_{\min}}$) for water waves:

$$u_{*_1} w_{a_1} > c_{p_{\min}} \quad \text{or} \quad u_{*_2} w_{a_2} > c_{p_{\min}},$$

surface waves exist, (26a)

$$u_{*_1} w_{a_1} < c_{p_{\min}} \quad \text{and} \quad u_{*_2} w_{a_2} < c_{p_{\min}},$$

surface waves do not exist. (26b)

The minimum phase speed for surface waves is

$$c_{p_{\min}} = (4g\sigma/\rho_w)^{1/4}, \quad (27)$$

which is approximately equal to 23 cm s^{-1}. The wind speed corresponding to the capillary cutoff is dependent on the relation between z_0 and u_*. For the BVW model, with $b = 0.18$ (Wu 1968), the cutoff is $U_{10} = 2.0 \pm 0.05$ m s^{-1}; however, with $b = 0.06$ (the value determined in section 4) the cutoff becomes $U_{10} = 1.8 \pm 0.05$ m s^{-1}.

The parameterization of roughness length for capillary waves generated through wave–wave interaction may be different from that of capillary waves generated through wind–wave interaction. This modeled capillary cutoff applies only to wind-generated capillary waves. Radar observations of the sea surface indicate that, in the presence of swell, parasitic capillary waves can exist at wind speeds less than that of the cutoff for conditions of local equilibrium (D. E. Weissman 1996, personal communication).

e. Summary of roughness length parameterization

In summary, the BVW momentum roughness length parameterization is

$$z_{0_i} = \beta'_\nu \frac{0.11\nu}{|\mathbf{u}_{*_i}|} + \left[\left(\beta'_c \beta_{c_i} \frac{b\sigma}{\rho_w |\mathbf{u}_{*_i}||\mathbf{u}_{*_i} \cdot \hat{\mathbf{e}}_i|}\right)^2 + \left(\beta'_g \frac{0.48}{w_{a_i}} \frac{|\mathbf{u}_{*_i}||\mathbf{u}_{*_i} \cdot \hat{\mathbf{e}}_i|}{g}\right)^2\right]^{0.5}, \quad (28)$$

where $\hat{\mathbf{e}}_1$ is parallel to the direction of wave propagation,

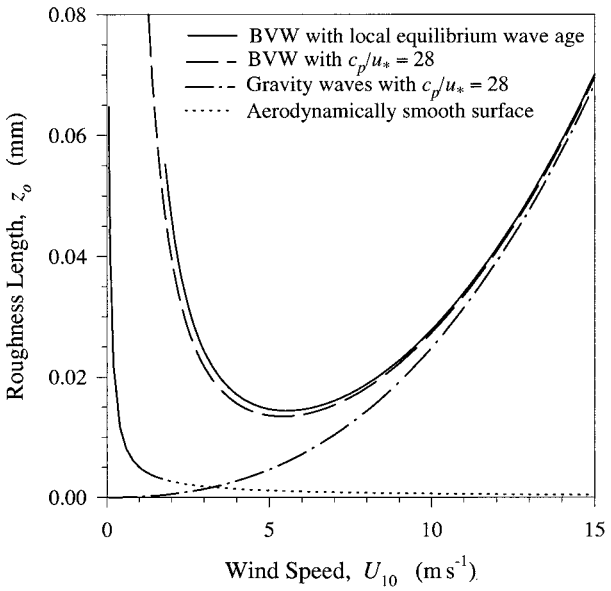

FIG. 1. Momentum roughness length parameterizations as a function of U_{10}.

and $\hat{\mathbf{e}}_2$ is perpendicular to $\hat{\mathbf{e}}_1$. For point fluxes, the β' values are equal to unity if the corresponding type of surface is contributing to the roughness length, and equal to zero if that type of surface is not contributing to the roughness length. The wave age for flow parallel to the direction of wave propagation can be associated with wave evolution (e.g., growing waves or swell), whereas the wave age for $\hat{\mathbf{e}}_2$ is always assumed to be that for local equilibrium.

The momentum roughness length components that have been discussed herein are shown in Fig. 1 as functions of U_{10} for conditions of neutral atmospheric stability. A wave age equal to 28 (corresponding to a fully developed sea), has been assumed for all curves except that labeled ''BVW with local equilibrium wave age,'' for which the wave age for local equilibrium was determined with a Phillips sea state parameterization, where the ratio of $U(H_s)$ to the mean wind speed over the crest is set at 0.82 (based on the imposed requirement of $c_p/u_* \approx 28$ for $U_{10} > 7$ m s^{-1}; Bourassa et al. 1998, submitted to *J. Phys. Oceanogr.*). Both BVW roughness lengths are calculated for parallel wind, surface currents, and wave propagation. The differences in roughness length between the BVW parameterization with $w_a = 28$ and w_a determined by the equilibrium sea state parameterization are shown to be small for high wind speeds, but the differences can be large for light winds, where the capillary cutoff changes from 1.8 m s^{-1} for the equilibrium sea state parameterization to an unrealistically low value of 0.8 m s^{-1} when $w_a = 28$ is assumed. The discontinuities in the roughness length for the BVW curves correspond to this capillary cutoff, and are due to the assumption of local wind-wave equilibrium: the discontinuity is analogous to the jump in stored energy as a function of temperature when H_2O changes phase from water to vapor. For U_{10} between the capillary cutoff and approximately 5 m s^{-1}, the roughness length determined with the BVW model is much greater than that of the Smith (1988) and Smith et al. (1992) parameterizations. The differences arise because neither the Smith (1988) nor Smith et al. (1992) parameterizations are based on observations within this range of wind speeds (they are based on higher wind speed observations), and neither parameterization considers capillary waves as roughness elements. Furthermore, the Smith (1988) parameterization is based on open ocean observations: they are likely to be confounded by swell and complex sea states, which reduces the roughness length approximately a factor of three.

4. Reanalysis of the dimensionless constant in the capillary wave component of roughness length

The values of modeled stress and latent heat flux predicted using Wu's (1968, 1994) value of $b = 0.18$ are sufficiently large to suggest that capillary waves play a major roll in the fluxes governing the tropical general circulation. Systematic overpredictions of modeled fluxes compared to observations (Bradley et al. 1991, 1993) lead to consideration of shortcomings in the BVW roughness length parameterization, which included a reexamination of the original value of the b (Wu 1968). A second reason for reanalyzing b is that the value determined from Wu's wave tank observations did not consider the frame of reference modification: the fetch was assumed to be sufficiently short that gravity waves were negligible. A third reason to reconsider the determination of u_* and z_0 by traditional wave tank log-profile techniques (Wu 1968, 1975; Kusaba and Masuda 1988) is that u_* determined through eddy correlation techniques is systematically inconsistent with the u_* from traditional wave tank log-profile methods. This problem is demonstrated in section 4a; large systematic differences imply an error. In section 4a the wave tank value of b will be reexamined, and in the following section b will be estimated from field observations; these results are consistent, and they differ from Wu's original value.

Wu (1994) attempted to verify that, for U_{10} less than approximately 8 m s^{-1}, stresses determined with a roughness length from Eq. (16) were consistent with observations. Modeled neutral drag coefficients were compared to drag coefficients observed by Bradley et al. (1991). Wu found good matches and concluded that his value of $b = 0.18$ was reasonable. However, he failed to realize that most of the field observations were associated with highly unstable boundary layers (Bradley et al. 1991). The drag coefficients for highly unstable conditions are much greater than those for a neutral atmosphere. Consequently, the close fit between the modeled neutral drag coefficients and those observed

TABLE 2. Here U is the core wind speed in the wave tank, H_o is the significant wave height of mechanically generated waves (moving in the same direction as the wind), H is the significant wave height of the combined wind and mechanically induced waves, T_o is the period of the mechanically induced waves, u_{*EC} is the friction velocity determined by the eddy correlation technique, u_* is the friction velocity determined from a log-profile technique (the subscript $d = 0$ indicates values determined with the assumption that displacement height is negligible, and a subscript d indicates values determined without the assumption that displacement height is equal to zero), and ε is the error in log-profile friction velocity assuming that the eddy correlation value is correct.

U (m s^{-1})	H_o (m)	H (m)	T_o (s^{-1})	u_{*EC} (cm s^{-1})	$u_{*d=0}$ (cm s^{-1})	$\varepsilon_{d=0}$ (%)	$z_{od=0}$ (μm)	u_{*d} (cm s^{-1})	ε_d (%)	z_{od} (μm)	d (mm)
2.19	0	0.48	NA	8.9	13.5	52	309	9.5	8	39	11
4.60	0	1.75	NA	19.0	23.0	21	84.5	17.9	−6	90	20
2.11	2.23	2.44	0.80	9.1	14.1	55	592	9.8	8	74	18

for highly unstable conditions indicates that Wu's $b = 0.18$ overestimates the neutral stress.

a. Reevaluation of wave tank observations

Our technique for determining u_* and z_0 differs from traditional wave tank applications of the profile technique in that we consider the importance of surface current and displacement height (d) in deriving u_* and z_0. The displacement height is a vertical offset of the logarithmic profile (Covey 1983; Stull 1988): z in Eq. (2) is replaced with $z - d$. Both U_s and d are negligible when a known relation between u_* and z_0 is used to determine $U(z \gg d)$, u_*, or z_0 from theory; however, they are not negligible when the profile method is used to determine u_* and z_0 (Covey 1983; Stull 1988). Covey's (1983) technique is used to determine u_*, z_0, and d, where U is replaced by $U - U_s$. Wu's (1968) observed values of U and z are obtained from his Fig. 6, and the surface currents from his Fig. 3. Several of Wu's near-surface observations were in a region that is not characterized by a log-profile (Large et al. 1995); these observations are not used herein to determine log-profile parameters.

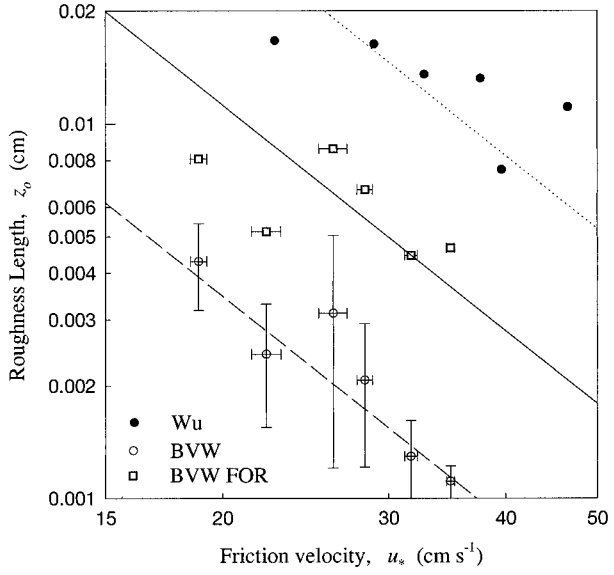

FIG. 2. Relation between roughness length and friction velocity. The error bars are 95% confidence limits. The dotted line is Wu's (1968) best fit with a slope of −2, the dashed line is the best fit to the revised u_* and z_0 prior to removing the frame of reference (FOR) modification, and the solid line is the fit with a slope of −2 to the revised u_* and z_0 after removing the frame of reference modification.

The importance of displacement height in determining log-profile values of u_* and z_0 is demonstrated with observations from the wind–wave-current facility at the University of Delaware's Air–Sea Interaction Laboratory. Profiles of mean wind speed were measured and for the same conditions that friction velocity was determined through the eddy correlation method (Tseng 1987). Measurements from one instrument were used in the eddy correlation and profile methods: fluctuating wind velocities (and mean winds) were determined with a hot-film anemometer. The friction velocities determined from the eddy correlation method and both profile methods are listed in Table 2. The errors in profile methods' friction velocities (assuming the eddy correlation values are correct) are given by $\varepsilon_{d=0}$ (average of +43% when d is assumed to equal zero) and ε_d (average of 3% when displacement height is considered). The rms percentage differences in friction velocity are 45% and 7%, respectively. The differences in z_0 between the two profile methods are large: in two of the three examples there are an order of magnitude difference in roughness length. Proper consideration of displacement height greatly reduces errors in log-profile values of friction velocity and roughness length.

Our values of u_* and z_0 are compared to Wu's values in Fig. 2, and are shown to be much smaller. The error bars represent the 95% confidence interval (two standard deviations determined by Covey's method): the relative uncertainty (expressed as one standard deviation) in u_* is approximately 1%, and that in z_0 is approximately 10%. Therefore, Wu's values are 10 to 1000 standard deviations greater than our values: the differences are very large in comparison to our accuracy. The dotted line in Fig. 2 represents Eq. (16) with Wu's $b = 0.18$, and the dashed line is the best-fit line through our u_* and z_0 values. The slope of our line is -2.1 ± 0.2 (one standard deviation), the y intercept is -13.5 ± 0.4, and the $r^2 = 0.84$. The value of b (prior to removing the frame of reference modification to z_0) is a function of the y intercept (B):

$$b = \rho_w e^B/\sigma, \tag{29}$$

which results in $b = 0.019$ with confidence limits of 0.013 and 0.027 (a factor of 1.4) corresponding to ± 1 standard deviation in *B.* Clayson et al. (1996) used this value of *b,* without a frame of reference modification, and showed that the biases between modeled and observed stress were small and that the bias was independent of wind speed. The Clayson et al. roughness length is almost equivalent to the BVW roughness length when the mean motions are assumed to be parallel and the waves are assumed to be in local equilibrium with the wind.

The frame of reference modification may be responsible for a portion of the large variances from mean observed fluxes, as well as an additional explanation for how sea state contributes to differences in z_0 between field and wave tank observations. The frame of reference modification reduced the values of z_0 calculated from the wave tank velocity profiles. It is presumed that the relationship between z_0 and u_* in (16) applies to roughness lengths that have not been modified to the frame of reference of the surface current. These roughness lengths can be calculated by inverting (24). The values of T_p and H_s are taken from Wu's Fig. 4. The resulting roughness lengths are shown as squares in Fig. 2; uncertainties in z_0 are not shown because uncertainties in T_p and H_s are unknown. The *y* intercept is found for the best-fit line with a slope of -2 (the solid line in Fig. 2), and *b* is found to equal 0.06 (which is used throughout this study). This value is approximately one-third of Wu's original value. In the next section, it will be shown that this value of *b* is similar to the value determined from field observations.

b. Capillary wave roughness in SCOPE observations

Observations from the San Clemente Ocean Probing Experiment (SCOPE; Fairall et al. 1996a) were used to test the model for extremely old age seas. These observations were taken from the Scripps Institute Floating Instrument Platform: R/P *FLIP.* The advantage of the SCOPE dataset over the Coupled Ocean–Atmosphere Response Experiment (COARE) datasets is that SCOPE observations include the dominant wave phase speed. Consequently, there is no need for any assumptions about wave age or local wind–wave equilibrium. The SCOPE phase speeds and wave ages (Fig. 3) are extremely large compared to local equilibrium values; therefore, the influence of capillary waves is emphasized. The greatest difficulty with SCOPE data is that the angle between the direction of wave propagation and the wind was not recorded in the available dataset, other than the qualitative statement that the angle was often large. The SCOPE observations were kindly provided by Chris Fairall.

Observations from SCOPE were used to determine the value of *b* required for the model to match the observations. Observed wind speeds, phase speeds, temperatures, and humidities were used as input; the values of *b* were chosen to match the measured friction velocities. Observations of the direction of wave propagation were unavailable; therefore, it was assumed that the waves propagated parallel to the winds. For 5 of the 131 cases it was found that $b = 0$, indicating that capillary waves were not present. For most of the cases, the values of *b* were between 0.02 and 0.3. The geometric average of the values is 0.05 with confidence limits of 0.04 and 0.06 (a factor of 1.2). This value of *b* is one standard deviation (of the field value) lower than the value determined from the laboratory observations. More detailed field observations, including vector stresses and the direction of wave propagation, will be required before field observations can be used to make a more accurate evaluation of *b.* Nevertheless, the near-consistency between laboratory and field observations strongly supports the concepts of capillary wave roughness and frames of reference used to develop the BVW model.

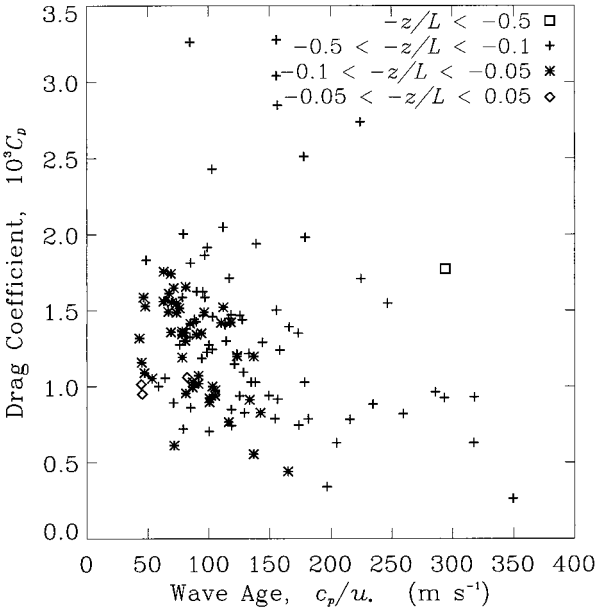

FIG. 3. SCOPE C_D as a function of wave age (c_p/u_*) and the nondimensional atmospheric stability parameter (z/L).

5. Influence of frame of reference and direction of wave propagation

The relative importance of capillary waves, the frame of reference modifications, and the angle (θ) between the direction of wave propagation and the direction the wind is moving, are functions of wind speed. The influences of capillary waves and the frame of reference modification (which is closely related to capillary waves) are relatively great for wind speeds slightly greater than the capillary cutoff, and the relative im-

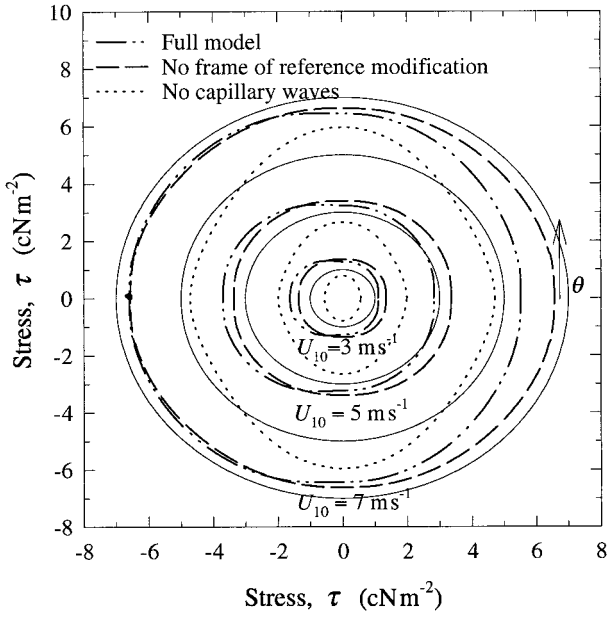

FIG. 4. Neutral stress magnitudes, as a function of the angle between the direction of the wind and the direction of wave propagation, for three wind speeds (3, 5, and 7 m s^{-1}). The swell has a phase speed of 20 m s^{-1}. The dotted line indicates the stress ignoring capillary waves, the dashed line indicates the stress ignoring the frame of reference correction, and the dash–dot–dot line shows both considerations. The solid lines show stresses of 1, 3, 5, and 7 cN m^{-2}.

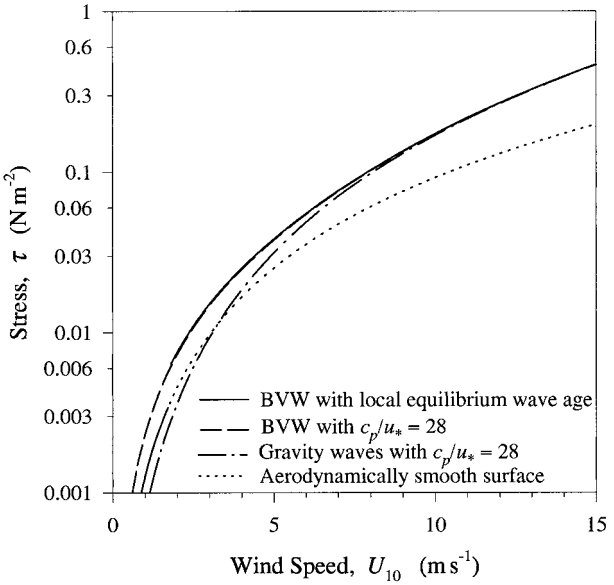

FIG. 5. Neutral stress for various parameterizations as a function of U_{10}.

portance of these influences decreases as wind speed increases. The magnitude of the modeled neutral stress is shown (Fig. 4) as a function of the angle θ, for swell with a dominant phase speed of 20 m s^{-1}, with U_{10} = 3, 5, and 7 m s^{-1}. The wind and waves move in parallel directions ($\theta = 0$) on the positive x axis, and θ increases in the counterclockwise direction. The inner rings represent the U_{10} = 3 m s^{-1} cases, the middle set is for U_{10} = 5 m s^{-1}, and the outer set is for U_{10} = 7 m s^{-1}. The dotted rings show the stresses when capillary waves and the frame of reference modification are ignored, the dashed lines show stress with capillary wave roughness and without frame of reference modifications, and the dash–dot–dot lines show stresses with both considerations. For each of the wind speeds, the stresses modeled without capillary waves (dotted lines) are smaller in magnitude than the stresses modeled with capillary waves; however, the fraction of stress associated with capillary waves decreases as the wind speed increases.

Without the frame of reference correction the stresses are symmetric about the axis of wave propagation ($\hat{\mathbf{e}}_1$) and the perpendicular axis ($\hat{\mathbf{e}}_2$). The symmetry about $\hat{\mathbf{e}}_2$ is lost when the frame of reference modification is applied. The influence of the frame of reference modifications is more evident at low wind speeds because this modification is applied solely to the roughness length for capillary waves, which is the dominant roughness at these wind speeds (a frame of reference modification for gravity waves is discussed in section 8c). For a fixed wind speed, the dependence on θ is such that the stress (and C_D) is least when the mean wind parallels the direction of wave propagation, it is greater when $\theta = 90°$, and greatest when $\theta = 180°$. This result is consistent with the observations of Donelan et al. (1997). For the U_{10} = 3 m s^{-1} example (Fig. 4), the stress when wind is moving parallel to the direction of wave propagation is 82% of the stress when the wind is moving in the opposite direction. This ratio is 87% for U_{10} = 5 m s^{-1}, and it is 91% for U_{10} = 7 m s^{-1}. The percentage differences in stress decrease as the wind speed increases; however, the magnitude of the difference increases as the wind speed increases (see Fig. 4). The influence of the frame of reference correction increases as the ratio of the ''orbital velocity to the friction velocity'' increases.

6. Neutral components of modeled fluxes

In order to demonstrate the impact of capillary waves in a manner that is unbiased by parameterizations of atmospheric stability, and which is consistent with the bulk of the literature, the neutral components of the modeled stress and drag coefficients are shown for winds that are parallel to the direction of wave propagation. The influence of capillary waves will be apparent as the difference between the one-dimensional BVW values and the purely gravity wave values.

a. Stress

The BVW stress is similar to that of the gravity wave-based parameterizations (Charnock 1955; Smith 1988; Smith et al. 1992) for $U_{10} > 7$ m s^{-1} (Fig. 5); however,

for $U_{10} < 5$ m s^{-1}, capillary waves can make important contributions to the stress. The mean winds in the Tropics are typically between 1 and 5 m s^{-1}. Therefore, tropical stresses and wind-induced currents are often underestimated. The local influence of this increase in stress is probably small; however, when the increase is integrated over that area of the Tropics the cumulative effect is likely to have an important impact on the tropical general circulation.

Wave age has little effect on the stress for $U_{10} < 7$ m s^{-1} except to alter the value of the capillary cutoff for wind-induced capillary waves. Wave ages as large as 120 have been observed in the Tropics (Deleonibus 1972) and off of the California coast (Fairall et al. 1996a); the corresponding cutoff is 0.4 m s^{-1}, which is much less than $U_{10} = 1.8$ m s^{-1} for the BVW model with equilibrium wave age. Some caution must be used when applying Eq. (14) to wave ages greater than 30 because the gravity wave roughness length parameterization has not been verified for such conditions. Nevertheless, due to the influence of sea state on the capillary cutoff, it is clear that the model indicates that sea state (directional information as well as wave age) is an important parameter at low wind speeds as well as at high wind speeds.

b. Drag coefficients

The BVW neutral drag coefficients (C_{DN})

$$C_D = u_*^2/U^2 \tag{30}$$

for $U_{\text{cutoff}} < U_{10} < 6$ m s^{-1} are much larger than those for models that do not consider capillary waves (Fig. 8). Results are shown for a variety of wave ages, as well as for local equilibrium (dashed curve). There are relatively few neutral drag coefficients determined from observations with $U_{10} < 7$ m s^{-1}: Large and Pond (1981; dot–dash curve) found $C_{DN} = 1.2 \times 10^{-3}$ for $U_{\text{cutoff}} < U_{10} < 6$ m s^{-1} in the open ocean; and Bradley et al. (1991) found $C_{DN} = 1.3 \times 10^{-3}$ near $U_{10} = 2$ m s^{-1}, and $C_{DN} = 1.16 \times 10^{-3}$ near 4 m s^{-1}. For winds near 1 m s^{-1}, Bradley et al. found C_{DN} to be near 2.5×10^{-3}. An empirical $C_{DN}(U_{10})$ (Large et al. 1995) combining the results of Large and Pond with a GCM-based fit for low wind speed is shown as the dot–dot–dot–dash curve. The mean $C_{DN}(U_{10})$ from the Surface of the Ocean, Fluxes and Interactions with the Atmosphere (SOFIA), and Structures des Echanges Mer-Atmosphere, Proprietes des Heterogeneities Oceaniques: recherche Experimentale (SEMAPHORE) experiments (Dupuis et al. 1997) is shown as the dotted line. The location of the minima in this curve is consistent with the BVW $C_{DN}(U_{10})$; models combining an aerodynamically smooth surface with gravity waves predict a minima near 2.3 m s^{-1}. All these observations and empirical relations are consistent with the BVW model predictions for long swell, which is typical of the open ocean and presumably consistent with many of these observations. These observed drag coefficients are much larger than would be expected for an aerodynamically smooth surface, which is often assumed in the calculation of stress for low wind speeds.

The sensitivity of the drag coefficient to wave age is relatively low for lower wind speeds and older seas. In section 5, and in the observations of Donelan et al. (1997), it was shown that for these conditions there is considerable variation in the drag coefficient due to the angle between the mean wind and the mean direction of wave propagation. These results are consistent with the observations that open ocean drag coefficients (old seas with swell from multiple sources) have little apparent dependence on wave age (e.g., Yelland et al. 1998). The consideration of directional aspects of sea state is required to model most open ocean conditions.

c. Sensible and latent heat fluxes

The neutral terms of the modeled sensible and latent heat fluxes (Figs. 6a,b) behave similarly to the corresponding neutral stress. The figures correspond to values of $T_{10} - T_s = 1.5$ K and 90% relative humidity, which are typical of tropical differences of temperature and moisture with height. Changes of less than 25 W m^{-2} in the sum of the latent and sensible heat fluxes have been shown to have a qualitative impact of the shape and strength of the European Centre for Medium-Range Weather Forecasts (ECMWF) GCM's tropical general circulation (Miller et al. 1992; Carrington and Anderson 1993). For low wind speed regions, such as the Tropics, the results shown in Fig. 6 suggest that increases in fluxes due to capillary waves can be of similar magnitude. The version of the ECMWF model discussed in the above studies had a Charnock roughness length parameterization, which is similar to the curve (Fig. 6) for "gravity waves with $c_p/u_* = 28$." The curves in Fig. 6, which include fluxes for an aerodynamically smooth surface and for gravity waves, provide an indication of the impact of capillary waves. The impact of capillary waves will be larger for nonneutral fluxes (section 7b), and may be sufficiently large to have a substantial effect on the tropical general circulation.

7. Comparison to observations

Field data from SCOPE are used to evaluate the modeled drag coefficients. The mean influences of capillary waves on nonneutral fluxes of momentum, heat, and moisture are also examined (section 7b). It has already been shown that the model predicts larger drag coefficients than are expected for aerodynamically smooth flow. Observations from SCOPE, SOFIA, and SEMAPHORE experiments find larger drag coefficients than are expected for aerodynamically smooth flow. In section 7a it will be shown that the consideration of capillary waves improves the accuracy of modeled drag coefficients. The influence of capillary waves is compared to that of boundary layer convection in section

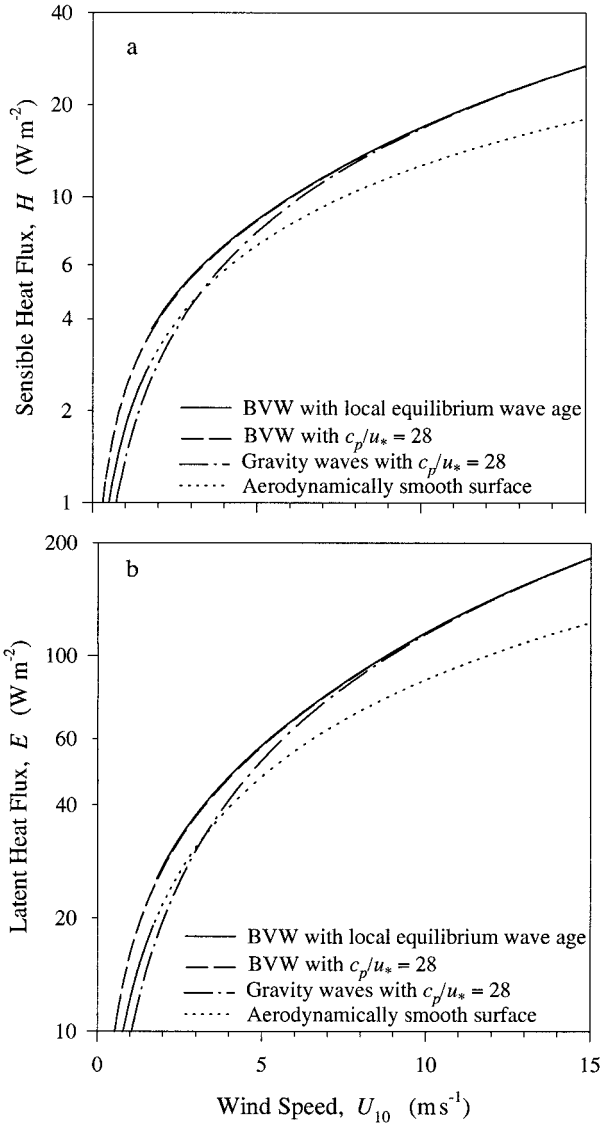

FIG. 6. Neutral sensible and latent heat fluxes for various parameterizations as a function of U_{10}.

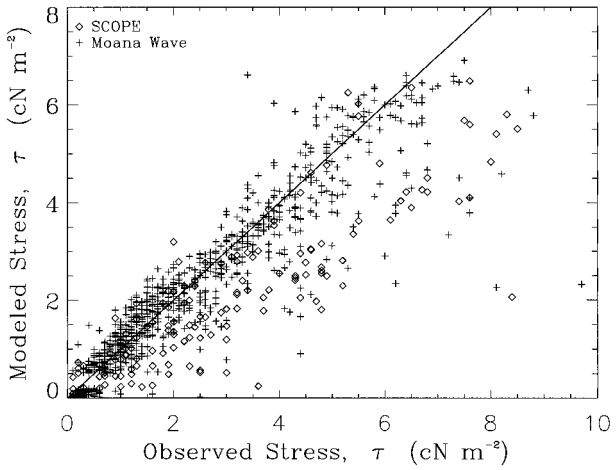

FIG. 7. Comparison of modeled stresses to observations from SCOPE and the R/V *Moana Wave*. The solid line shows a perfect match.

8a. It will be shown that the effect of capillary waves on heat fluxes is of the order shown to be significant (Miller et al. 1992; Carrington and Anderson 1993) in GCMs.

a. Accuracy of various models

All of the roughness length parameterizations discussed herein accurately model the general trend of increasing stress with increasing wind speed. In the case of the SCOPE data the linear correlation coefficients between modeled and observed stresses (for $0 < U_{10} < 7$ m s^{-1}) are 0.86 ± 0.01; indicating similar accuracy in the models' predictions of the trend in the change of stress with wind speed. A comparison of modeled stresses and observed stresses (Fig. 7) indicates that the modeled stresses are usually within 0.01 N m^{-2} of the observed stresses. The vast majority of larger differences show the modeled stress underestimating the observations. Neither the SCOPE nor the R/V *Moana Wave* datasets include the direction of the wind relative to the direction of propagation of the dominant waves. This absence, coupled with the observations of Donelan et al. (1997) and the modeling in section 5, suggests that the larger underestimations of the model could be due to winds, waves, and currents that do not have parallel mean motion vectors.

The drag coefficient has relatively little dependence on wind speed (Fig. 8) for $2 < U_{10} < 6$ m s^{-1}: the wind speed dependent trend is tiny in comparison to that of stress. However, the use of C_D rather than stress does not remove the influence of sea state (Donelan et al. 1997): wave age and differences in direction of wind and wave propagation result in additional variability in C_D. The correlation between drag coefficients is a much better indication of a model's capability in predicting departures from the trend. As indicated earlier, the uncertainty in the direction of wave propagation is likely to be responsible for a large fraction of the variation in the drag coefficients. Nevertheless, it will be shown that the accuracy of the modeled drag coefficients improves for the models with more detailed physical considerations, despite the assumption of parallel wind and wave propagation vectors. The BVW model without capillary waves ($\beta_c' = 0$, and $\mathbf{U}//\mathbf{U}_s//\mathbf{e}_1$; similar to Smith et al. 1992) has a poor correlation ($r = -0.20$) to SCOPE observations; the negative value indicates that increases (decreases) in modeled C_D are associated with decreases (increases) in the observed C_D. The Smith (1988) parameterization, which considers the roughness length to be the sum of the roughness lengths for gravity waves and an aerodynamically smooth surface, has a correlation coefficient of 0.15. Despite this low correlation,

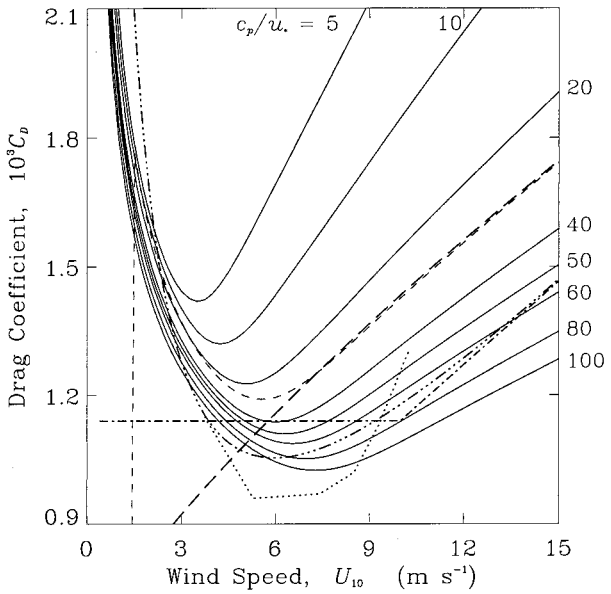

FIG. 8. Neutral drag coefficients for various wave ages (c_p/u_*), assuming the mean wind direction is parallel the mean direction of wave propagation. The values of wave age corresponding to the solid curves are given in the figure. The thin dashed curve is the modeled drag coefficients for wind–wave equilibrium ($c_p/u_* \approx 28$ for $U_{10} > 7$ m s^{-1}); the vertical dashed line indicates the capillary cutoff. The thick dashed curve shows the Smith et al. (1992) drag coefficients. The dotted curve is the best fit to the SOFIA and SEMAPHORE data (from Dupuis et al. 1997; their Fig. 3a). Also shown are two empirical drag coefficients for the open ocean: the dot–dash (·-·-) curve is Large and Pond (1981) and the dot–dot–dot–dash (···-) curve is Large et al. (1995).

the Smith (1988) parameterization is a great improvement ($\Delta r = 0.35$) over the base correlation of -0.20. The correlation with the BVW model is 0.31, which is a great improvement ($\Delta r = 0.51$) over the base value and doubles the correlation of the Smith (1988) parameterization. Clearly, more detailed observations will be required to further test and improve the modeled physics, particularly the anisotropic roughness length.

b. *Changes in magnitudes of modeled fluxes for tropical nonneutral conditions*

The changes in fluxes due to capillary waves are examined using three datasets from tropical field observations. One set is the SCOPE data, the second is Chris Fairall's Tropical Ocean Global Atmosphere (TOGA) COARE observations from the R/V *Moana Wave* (Fairall et al. 1996b), and the third set combines Frank Bradley's observations from the R/V *Franklin* (Bradley et al. 1991; Bradley et al. 1993). These datasets were chosen because they emphasize low wind speeds. Neither wave age nor phase speed observations were available with the observations from the *Moana Wave* and the *Franklin*; local equilibrium values of wave age, from the equilibrium sea state parameterization, were used to determine the fluxes. It is likely that swell was present

TABLE 3. Influence of capillary waves on fluxes. The first column shows mean observed values, the second shows the values with capillary waves, and the third column shows the values without capillary waves ($\beta_c' = 0$). The fourth column is the mean difference due to capillary waves, and the fifth is the mean percentage increase relative to the values without capillary waves.

	Obs	Mean with capillary waves	Mean without capillary waves	Change due to capillary waves	Percent change due to capillary waves
SCOPE					
$10^3 C_D$	1.42	1.20	0.87	0.33	42
τ (cN m^{-2})	3.99	3.39	2.73	0.66	42
H (W m^{-2})	14.9	13.9	12.4	1.5	16
E (W m^{-2})	63.5	58.8	53.2	6.6	16
Moana					
$10^3 C_D$	2.76	1.43	1.14	0.29	19
τ (cN m^{-2})	2.43	2.41	2.09	0.32	19
H (W m^{-2})	9.2	6.0	5.6	0.5	11
E (W m^{-2})	87.5	85.3	78.3	7.0	11
Franklin					
$10^3 C_D$	NA	1.42	1.04	0.38	37
τ (cN m^{-2})	NA	1.01	0.74	0.27	37
H (W m^{-2})	6.7	3.9	3.4	0.5	14
E (W m^{-2})	66.9	38.0	33.0	5.0	14

for most of the observations. Therefore, the local-equilibrium wave ages underestimate the true wave ages, which results in an underestimation of the importance of capillary waves. The observed winds, temperatures, humidities, and phase speeds (for SCOPE data) are used to model stresses, drag coefficients, sensible heat fluxes, and latent heat fluxes. Mean fluxes modeled with capillary waves are compared to observations and mean fluxes without capillary waves (Table 3). In all cases, consideration of capillary waves results in increases in the modeled drag coefficient and mean fluxes of momentum, heat, and moisture. Furthermore, the mean modeled result considering capillary waves are always a better match to the observations. The observations from the R/V *Franklin* do not include stresses because of difficulties removing ship motion from the winds used in the eddy correlation method (F. Bradley 1994, personal communication). The large differences between modeled heat fluxes and those observed from the R/V *Franklin* tend to be associated with low wind speeds. Improvement of the model through the inclusion of additional physics, such as differences between the skin temperature and observed temperature due to evaporative cooling and solar heating, increases the accuracy of modeled fluxes (Clayson et al. 1996). The physics discussed herein leads to improvements in the modeled stress, and the physics discussed by Clayson et al. improves the modeled fluxes in heat and moisture. Combining these improvements would lead to improved modeling of atmospheric stability, and consequently improvements in the modeled fluxes.

The capillary wave-related increases in modeled heat fluxes are sufficiently large that they would cause a qualitative change in the ECMWF's tropical general cir-

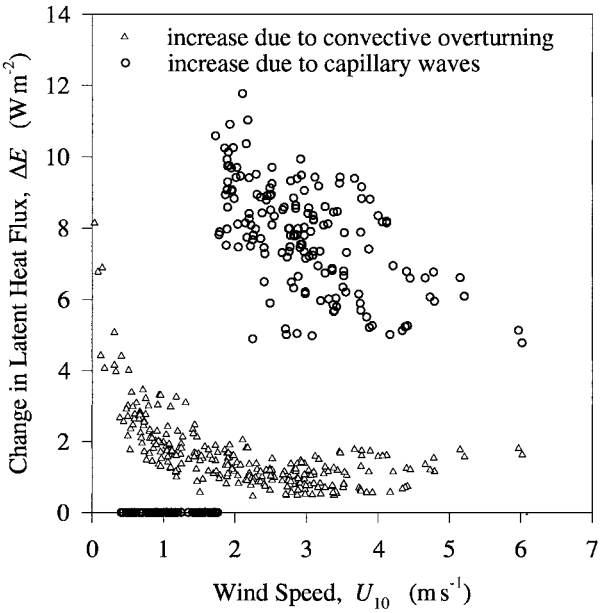

FIG. 9. Increased evaporation due to capillary waves (○) and convective overturning (△).

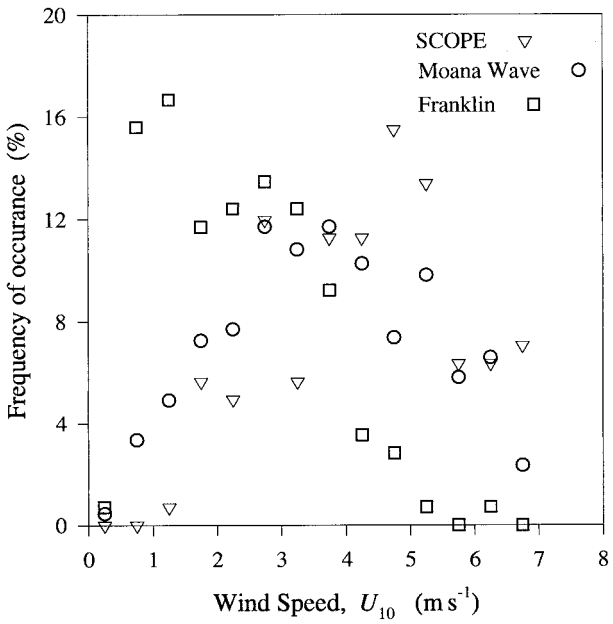

FIG. 10. Probability distribution functions of wind speed ($U_{10} < 7$ m s^{-1}) for the three datasets. Wind speed bins are 0.5 m s^{-1} wide.

culation. It is expected that these increases in fluxes are sufficiently large that there will also be qualitative changes in the results of GCMs with better representations of the Tropics.

8. Discussion

There are several suggested processes that contribute to an increased heat flux from the tropical oceans to the atmospheric boundary layer. One process is small-scale convection (or ''gustiness''). Another process is the heating of a shallow surface layer (Fairall et al. 1996b). There is a thin (order 10 cm) layer of warm water at the surface of relatively calm seas. The temperature at the top of this layer can be several degrees warmer than the temperature at depths of 2–6 m, where most ships intake water to measure the ''surface'' temperature. The approximation that the surface temperature is equal to the temperature at depth results in underestimated fluxes. The impact of a warm surface layer is difficult to compare to the impact of capillary waves: the temperature profile of the warm layer is dependent on the surface stress as well as the prior several hours of radiative heating. In contrast, the impact of gustiness is parameterized in terms of local parameters and can easily be compared to the impact of capillary waves.

a. Importance of capillary waves vs convection

Gustiness has been suggested by Fairall (Fairall et al. 1996b) to cause a large increase (~5 W m^{-2}) in heat fluxes for low wind speed fluxes ($U_{10} < 3$ m s^{-1}). A similar result is found when Fairall's gustiness parameterization [Eq. (7)] is applied in the calculation of latent heat fluxes for the *Franklin* observations (Fig. 9). Only a small fraction of observed wind speeds are sufficiently small that there are large increases due to gustiness. The probability distributions of wind speeds for the three datasets are shown in Fig. 10. The average changes in latent heat fluxes (Table 4) related to gustiness, for all wind speed observations less than 7 m s^{-1}, are between 0.9 and 2 W m^{-2}.

The increase in latent heat flux due to capillary waves is also a function of wind speed (Fig. 9). For wind speeds less than the capillary cutoff there are no changes in the fluxes. For wind speed near 2 m s^{-1} the increases are near 10 W m^{-2}, and the magnitudes of the changes are reduced as the wind speeds increase. The average change in latent heat flux (Table 4), for all wind speed observations less than 7 m s^{-1}, is between 4 and 9 W m^{-2}. The mean change in latent heat flux due to capillary waves is approximately three to six times larger than the increase due to convective overturning. Furthermore, the interaction between the two processes lowers the capillary cutoff and causes the mean increase in

TABLE 4. Changes in latent heat flux (W m^{-2}). The first row shows the change in latent heat flux when gustiness is neglected. The second row shows the change when capillary waves are neglected. The third row shows the change when both capillary waves and gustiness are considered.

	SCOPE	*Moana Wave*	*Franklin*
Capillary waves	6.7	7.1	4.6
Gustiness	0.9	1.8	1.4
Both	7.6	8.9	6.4

latent heat fluxes to be greater than the sum to the independent changes. Clearly, the increased heat flux due to capillary waves is more important than that due to convective processes.

b. Bulk flux applications of the BVW model

Bull fluxes represent transfers over large areas that may be nonhomogeneous, whereas point fluxes represent transfers over small homogeneous surfaces. For most low wind speeds ($U_{10} < 5$ m s^{-1}), large water surfaces cannot be described as being uniformly aerodynamically smooth or rough ($\beta' = 0$ or $\beta' = 1$). Such surfaces are patchy due in part to small-scale convection, and in part due to insufficient stress to maintain a rough surface. It is these features that smooth the discontinuity near the capillary cutoff in the point flux model. In such cases, the binary logic applied to the point flux model is an inadequate description of the surface. It is likely that fuzzy logic (McNeill and Frieburger 1993) can be applied to improve the description. With a fuzzy logic, the β' values correspond to the fraction of the surface covered with the corresponding type of roughness elements. There are two constraints:

$$\beta'_\nu + \beta'_g = 1 \quad \text{and} \tag{31}$$

$$\beta'_c \leq \beta'_g. \tag{32}$$

The first constraint indicates that the total surface area is equal to the area that is aerodynamically smooth plus the area with gravity waves. The second constraint results from the condition that in the open ocean capillary waves rarely exist in the absence of gravity waves (albeit very small gravity waves for low wind speeds). At this time, there are insufficient low wind speed flux observations to determine how these fuzzy weighting parameters vary as functions of wind speed and atmospheric stability.

Inhomogeneities on the ocean surface could serve to enhance convective processes. Smaller roughness lengths in regions without capillary waves will cause the atmospheric stability to be further from neutral: in unstable boundary layers convective processes will be enhanced. Furthermore, the greater stress over the rougher surface will reduce the influence of warm surface layers. Consequently, updrafts are expected over smooth patches, and downdrafts over the areas with capillary waves. The parameterization of the influence of surface inhomogeneities on convection will likely require knowledge of the fraction of the surface covered by each type of roughness element. These considerations are likely to be important in modeling the interactions between surface fluxes, boundary layer convection, and boundary layer stability.

c. Gravity wave and frame of reference

It seems likely that a frame of reference correction should also be applied to gravity waves; however, there is little observational evidence that can be used to determine such a relationship. There have been numerous suggestions (e.g., Munk 1955; Phillips 1977; Al-Zamadi and Hui 1984; Donelan 1990) that the ''natural'' frame of reference for gravity waves is that which moves with the phase speed of the gravity waves that interact with the airflow. Many of these suggestions are related to the concept of form drag due to the gravity waves, and the effectiveness of wave evolution models (e.g., Miles 1957; Komen et al. 1994) based on form drag.

A shortcoming of the inverse wave age form of the gravity wave roughness length is the indifference to whether or not the wind is blowing parallel or antiparallel to the direction of wave motion. There is only one frame of reference where the roughness length for symmetrical gravity waves should be independent of the direction of the wind: $U - c$, where c is the phase speed of the waves interacting with the wind. The transformation to a U_s frame of reference would then have an $\exp(-\kappa \mathbf{c} \cdot \hat{\mathbf{e}}_i/\mathbf{u}_{*_i})$ form. Recall that roughness length must be positive: a negative value of wave age is physically inconsistent. The exponential form does not suffer from this shortcoming. It is commonly assumed that there is sufficient similarity among gravity waves that integration over the spectra of phase speeds is not required, and that $\mathbf{c}$ can be treated as proportional to $\mathbf{c}_p$. If the $0.48/w_a$ is removed from (28), then β_g becomes

$$\beta_{g_i} = \exp(-\kappa \psi \mathbf{c}_p \cdot \hat{\mathbf{e}}_i/\mathbf{u}_{*_i}), \tag{33}$$

where ψ is the constant of proportionality between $\mathbf{c}$ and $\mathbf{c}_p$. If β_g is forced to equal $0.48/w_a$ for high wind speeds, then $\psi \approx 0.36$. This result is consistent with the transfer of wind momentum to waves that are slower and smaller than the dominant waves. Furthermore, the $0.48/w_a$ form does not allow for the observed large changes in C_D (up to a factor of two; W. G. Large 1997, personal communication) with rapid changes in wind direction; however, when (33) is used to determine a drag coefficient, a change in direction can result in a very large change in C_D. The sea state would react quickly to such strong forcing, and a time-averaged drag coefficient could be consistent with observed changes in C_D. Further examination of high wind speed data will be required to test the validity of (33).

9. Conclusions

We have developed an air–sea interaction model that uses an improved model of the surface roughness to more accurately estimate surface fluxes. The new considerations are roughness length related to capillary waves, a frame of reference correction to roughness length, an anisotropic roughness length, and a distinction between aerodynamically smooth and rough surfaces. The correlation between modeled and observed drag coefficients is better than a model (Smith et al. 1992) based purely on gravity wave roughness. The BVW parameterization estimates drag coefficients more

accurately than the other parameterizations that were examined, and it provides a physical basis for the shape of an effective empirical $C_D(U_{10})$ (Large et al. 1995) and the observations of Dupuis et al. (1997). The observed and modeled local minima in $C_D(U_{10})$ (for U_{10} greater than the capillary cutoff) occur near 6 m s^{-1}, rather than near 2.3 m s^{-1}, which would be expected if capillary waves were insignificant. A large fraction of surface winds are within the range influenced by capillary waves; consequently, these improvements should often be useful in modeling air–sea interaction.

The influence of capillary waves on fluxes is smaller than originally expected because Wu's estimate of b, the dimensionless coefficient in the relation between capillary wave momentum roughness length and friction velocity, was one order of magnitude too large. The value of b was recalculated, and adjusted for frame of reference, using Wu's original wave tank data and a more thorough analysis technique, and it was found to be 0.06. The value of b was also determined from field observations and it was found to be 0.05 ± 0.01, which is consistent with the wave tank observations.

The magnitude of the influence of capillary waves was compared to that of boundary layer convective overturning. Both considerations could increase latent heat flux by up to 15/s W m^{-2}; however, these increase are a strong function of wind speed, with the presence of swell also playing important roles in determining the capillary cutoff. Convective processes increase the flux by an average of 1 W m^{-2}, except for very low wind speeds ($U_{10} < 1$ m s^{-1}), where the increases are nearer to 4 W m^{-2}. The increased latent heat flux due to capillary waves is approximately 10 W m^{-2} near the capillary cutoff and approximately 6 W m^{-2} near $U_{10} = 4$ m s^{-1}. In the Tropics, the winds are typically greater than the capillary cutoff and less than 5 m s^{-1}, indicating that the increase in fluxes due to capillary waves usually has a much greater effect than that of convective overturning.

The mean increase in fluxes due to capillary waves, estimated from observations taken on the R/P *FLIP*, R/V *Moana Wave*, and R/V *Franklin*, were 1 W m^{-2} in sensible heat, 6 W m^{-2} in latent heat, and 4×10^{-3} N m^{-2} in stress. These increases in stress and heat fluxes are sufficiently large to significantly modify topical circulation patterns in general circulation models.

New considerations in the BVW model make the model compatible with an extremely wide range of observations. The model is consistent with the open ocean observations for moderate and high wind speeds (Large and Pond 1981; Smith 1980; Anderson 1983; Dobson et al. 1994); through the consideration of sea state and capillary waves. The open ocean observations for low wind speeds in SCOPE (Fairall et al. 1994) and the SOFIA and SEMAPHORE experiments (Dupuis et al. 1997) requires the consideration of capillary waves and a very old sea state. For observations without swell (HEXOS; Smith et al. 1992), the observations are matched when a near-equilibrium sea state is used in the model. For conditions of nonequilibrium (wave tanks and SCOPE) the key considerations are capillary waves, sea state, and the frame of reference. The observed dependence of nonequilibrium C_{DN} on the angle between the mean directions of swell propagation and the wind (Donelan et al. 1997) requires the additional consideration of an anisotropic roughness length. The key change in GCMs and observational practices required to take advantage of these improvements in modeling is consideration of the two-dimensional sea state.

Acknowledgments. We thank John T. Snow, William G. Large, Carol Anne Clayson, James J. O'Brien, and anonymous reviewers for helpful discussions. We also thank Chris Fairall for providing the SCOPE and R/V *Moana Wave* observations, Frank Bradley for supplying the R/V *Franklin* observations, and the many people who took part in gathering and processing these observations. The research that produced this paper was primarily supported by the National Air and Space Administration under Grant NAG8-836, with partial support from the National Science Foundation under Grant ATM-9200534. Both grants were issued to Dr. Dayton Vincent at Purdue University. COAPS receives it base funding from the Secretary of Navy Grant from ONR to Dr. James J. O'Brien. Current funding is from the NASA JPL NSCAT Project.

REFERENCES

Al-Zanadi, M. A., and W. H. Hui, 1984: Turbulent air-flow over water waves—A numerical study. *J. Fluid Mech.,* **148,** 225–246.

Anderson, R. J., 1993: A study of wind stress and heat flux over the open ocean by the inertial dissipation method. *J. Phys. Oceanogr.,* **23,** 2153–2161.

Banner, M. L., and O. M. Phillips, 1974: On the incipient breaking of small scale waves. *J. Fluid Mech.,* **65,** 647–656.

Beljaars, A. C. M., and A. A. M. Holtslag, 1991: Flux parameterization over land surfaces for atmospheric models. *J. Appl. Meteor.,* **30,** 327–341.

Benoit, R., 1977: On the integral of the surface layer profile-gradient functions. *J. Appl. Meteor.,* **16,** 859–860.

Bourassa, M. A., 1993: An air–sea interaction model for stress, sensible heat, latent heat, and sea state, applicable to the full range of wind speeds. Ph.D. thesis, Purdue University, 97 pp.

Bradley, E. F., P. A. Coppin, and J. S. Godfrey, 1991: Measurements of sensible heat flux in the western equatorial Pacific Ocean. *J. Geophys. Res.,* **96,** 3375–3389.

——, J. S. Godfrey, P. A. Coppin, and J. A. Butt, 1993: Observations of net heat flux into the surface mixed layer of the western equatorial Pacific Ocean. *J. Geophys. Res.,* **98,** 22 521–22 532.

Brutsaert, W. A., 1982: *Evaporation into the Atmosphere.* Reidel, 299 pp.

Byushev, V. I., and O. A. Kuznetsov, 1969: Stuktrunye kharakteristiki atmosfernoi turbulentnosti v privodnom sloe nad otkrytym okeanom. Izvestiya AN USSR. *Fiz. Atmos. Okeana,* **5,** 327–332.

Carl, D. M., T. C. Tarbell, and H. A. Pankofsky, 1973: *J. Atmos. Sci.,* **30,** 788–794.

Carrington, D. J., and D. L. T. Anderson, 1993: Using an ocean model to validate ECMWF heat fluxes. *Quart. J. Roy. Meteor. Soc.,* **119,** 1003–1021.

Charnock, H., 1955: Wind stress on a water surface. *Quart. J. Roy. Meteor. Soc.,* **81,** 639–640.

Chou, S.-H., 1993: A comparison of airborne eddy correlation and bulk aerodynamic methods for ocean–air turbulent fluxes during cold-air outbreaks. *Bound.-Layer Meteor.,* **64,** 75–100.

Clayson, C. A., C. W. Fairall, and J. A. Curry, 1996: Evaluation of turbulent fluxes at the ocean surface using surface renewal theory. *J. Geophys. Res.,* **101,** 28 503–28 513.

Covey, W., 1983: A method for the computation of logarithmic wind profile parameters and their standard errors. Production Research Rep. 72, United States Department of Agriculture, 28–33.

Deleonibus, P. S., 1972: Momentum flux and wave spectra observations from an ocean tower. *J. Geophys. Res.,* **77,** 6506–6527.

Dobson, F. W., S. D. Smith, and R. J. Anderson, 1994: Measuring the relationship between wind stress and sea state in the open ocean in the presence of swell. *Atmos.-Ocean,* **32,** 327–356.

Donelan, M., 1990: Air–sea interactions. *The Sea,* B. LeMahaute and D. M. Hanes, Eds., John Wiley and Sons, Inc., 239–292.

——, W. M. Drennan, and K. B. Katsaros, 1997: The air–sea momentum flux in conditions of wind sea and swell. *J. Phys. Oceanogr.,* **27,** 2087–2099.

Dupuis, H., P. K. Taylor, A. Weill, and K. Katsoaros, 1997: Inertial dissipation method applied to derive turbulent fluxes over the ocean during the Surface of the Ocean, Fluxes and Interactions with the Atmosphere/Atlantic Stratocumulus Transition Experiment (SOFIA/ASTEX) and Structures des Echanges Mer-Atmosphere, Proprietes des Heterogeneities Oceaniques: Recherche Experimentale (SEMAPHORE) experiments with low to moderate wind speeds. *J. Geophys. Res.,* **102,** 21 115–21 129.

Dyer, A. J., 1974: A review of flux–profile relationships. *Bound.-Layer Meteor.,* **7,** 363–372.

Fairall, C. W., A. A. Grachev, A. J. Bedard, and R. T. Nishiyama, 1996a: Wind, wave, stress, and surface roughness relationships from turbulence measurements made on R/P FLIP in the SCOPE experiment. NOAA Tech. Memo. ERL ETL-268, 37 pp. [NTIS PB96-181334INZ.]

——, E. F. Bradley, D. P. Rogers, J. B. Edson, and G. S. Young, 1996b: Bulk parameterizations of air–sea fluxes for Topical Ocean Global Atmosphere Coupled Ocean–Atmosphere Response Experiment. *J. Geophys. Res.,* **101,** 3747–3764.

Geernaert, G. L., 1988: Measurements of the angle between the wind stress vector in the surface layer over the North Sea. *J. Geophys. Res.,* **91,** 7667–7679.

——, 1990: Bulk parameterizations for the wind stress and heat fluxes. *Surface Waves and Fluxes,* G. L. Geernaert and W. J. Plant, Eds., Vol. 1, Kluwer Academic Publishers, 336 pp.

Godfrey, J. S., and A. C. M. Beljaars, 1991: On the turbulent fluxes of buoyancy, heat and moisture at the air–sea interface at low wind speeds. *J. Geophys. Res.,* **96,** 22 043–22 048.

Komen., G. J., L. Cavaleri, M. Donelan, K. Hasselman, S. Hasselman, and P. A. E. M. Janssen, 1994: *Dynamics and Modeling of Ocean Waves.* Cambridge University Press, 532 pp.

Kondo, J., 1975: Air–sea bulk transfer coefficients in diabatic conditions. *Bound.-Layer Meteor.,* **9,** 91–112.

——, and H. Yamazawa, 1985: Aerodynamic roughness over an inhomogeneous ground surface. *Bound.-Layer Meteor.,* **35,** 331–348.

Kusaba, T., and A. Masuda, 1988: The roughness height and drag law over the water surface based on the hypothesis of local equilibrium. *J. Oceanogr. Soc. Japan,* **44,** 200–214.

Large, W. G., and S. Pond, 1981: Open ocean momentum flux measurements in moderate to strong winds. *J. Phys. Oceanogr.,* **11,** 324–336.

——, J. C. McWilliams, and S. C. Doney, 1994: Oceanic vertical mixing: A review and a model with nonlocal boundary layer parameterization. *Rev. Geophys.,* **32,** 363–403.

——, J. Morzel, and G. B. Crawford, 1995: Accounting for surface wave distortion of the marine wind profile in low-level ocean storms wind measurements. *J. Phys. Oceanogr.,* **25,** 2959–2971.

Lettau, H., 1969: Note on aerodynamic roughness-parameter estimation on the basis of roughness-element description. *J. Appl. Meteor.,* **8,** 828–832.

Liu, W. T., K. B. Katsaros, and J. A. Businger, 1979: Bulk parameterization of air–sea exchanges of heat and water vapor including the molecular constraints at the interface. *J. Atmos. Sci.,* **36,** 1722–1735.

Maat, M., C. Kraan, and W. A. Oost, 1991: The roughness of wind waves. *Bound.-Layer Meteor.,* **54,** 89–103.

McNeill, D., and P. Frieberger, 1993: *Fuzzy Logic.* Simon and Schuster, 319 pp.

Miles, J. W., 1957: On the generation of surface waves by turbulent shear flows. Part 2. *J. Fluid Mech.,* **6,** 568–582.

Miller, M. J., A. C. M. Beljaars, and T. N. Palmer, 1992: The sensitivity of the ECMWF model to the parameterization of evaporation over the tropical oceans. *J. Climate,* **5,** 418–434.

Munk, W. H., 1955: Wind stress on water: An hypothesis. *Quart. J. Roy. Meteor. Soc.,* **81,** 320–332.

Nikuradse, J., 1933: *Stromungsgesetze in rauben Rohren.* V. D. I. Forschungsheft 361, 22 pp.

Peilke, R. A., 1984: *Mesoscale Meteorological Modeling.* Academic Press, 165 pp.

Perrie, W., and B. Toulany, 1990: Fetch relations for wind-generated waves as a function of wind-stress scaling. *J. Phys. Oceanogr.,* **20,** 1666–1681.

Phillips, O. M., 1977: *The Dynamics of the Upper Ocean.* 2d ed. Cambridge University Press, 336 pp.

Rieder, K. F., J. A. Smith, and R. A. Weller, 1994: Observed directional characteristics of the wind, wind stress, and surface waves on the open ocean. *J. Geophys. Res.,* **99,** 22 589–22 596.

Schumann, U., 1988: Minimum friction velocity and heat transfer in the rough surface layer of a convective boundary layer. *Bound.-Layer Meteor.,* **44,** 311–326.

Smith, S. D., 1980: Wind stress and heat flux over the ocean in gale force winds. *J. Phys. Oceanogr.,* **10,** 709–726.

——, 1988: Coefficients for sea surface wind stress, heat flux, and wind profiles as a function of wind speed and temperature. *J. Geophys. Res.,* **93,** 15 467–15 472.

——, 1989: Water vapor flux at the sea surface. *Bound.-Layer Meteor.,* **47,** 277–293.

——, and Coauthors, 1992: Sea surface wind stress and drag coefficients: The HEXOS results. *Bound.-Layer Meteor,* **60,** 109–142.

Stull, R. B., 1988: Measurement and simulation. *An Introduction to Boundary Layer Meteorology,* Kluwer Academic Publishers, 405–440.

Toba, Y., N. Ida, H. Kawamura, N. Ebuchi, and I. S. F. Jones, 1990: Wave dependence of sea-surface wind stress. *J. Phys. Oceanogr.,* **20,** 705–721.

Trenberth, K. E., G. L. Large, and J. G. Olson, 1989: The effective drag coefficient for evaluating wind stress over oceans. *J. Climate,* **2,** 1507–1516.

Tseng, R.-S., 1987: Longitudinally-averaged and wave modulated turbulent boundary layers above and below a wave-disturbed water surface. Ph.D. thesis, University of Delaware, 183 pp.

Ursell, F., 1956: Wave generation by wind. *Surveys in Mechanics,* G. K. Batchelor and R. M. Davies, Eds., Cambridge University Press, 216–249.

Wu, J., 1968: Laboratory studies of wind–wave interactions. *J. Fluid Mech,* **34,** 91–111.

——, 1975: Wind-induced drift currents. *J. Fluid Mech.,* **68,** 49–70.

——, 1980: Wind-stress coefficients over sea surface near neutral conditions—A revisit. *J. Phys. Oceanogr.,* **10,** 727–740.

——, 1994: The sea surface is aerodynamically rough even under light winds. *Bound.-Layer Meteor.,* **69,** 149–158.

Yelland, M. J., B. I. Moast, P. K. Taylor, R. W. Pascal, J. Hutchings, and V. C. Cornell, 1998: Wind stress measurements from the open ocean corrected for airflow distortion by the ship. *J. Phys. Oceanogr.,* **28,** 1511–1526.